24 Jun 2024

Interpenetrated Lattices of Quaternary Chalcogenides Displaying Magnetic Frustration, High Na-Ion Conductivity, and Cation Redox in Na-Ion Batteries

Santhoshkumar Sundaramoorthy

Srikanth Balijapelly

Sudip Mohapatra

Sutapa Bhattacharya

et. al. For a complete list of authors, see https://scholarsmine.mst.edu/chem_facwork/4023

Recommended Citation

S. Sundaramoorthy et al., "Interpenetrated Lattices of Quaternary Chalcogenides Displaying Magnetic Frustration, High Na-Ion Conductivity, and Cation Redox in Na-Ion Batteries," *Inorganic Chemistry*, vol. 63, no. 25, pp. 11628 - 11638, American Chemical Society, Jun 2024.
The definitive version is available at https://doi.org/10.1021/acs.inorgchem.4c00927

Inorganic Chemistry

pubs.acs.org/IC

Article

Interpenetrated Lattices of Quaternary Chalcogenides Displaying Magnetic Frustration, High Na-Ion Conductivity, and Cation Redox in Na-Ion Batteries

Santhoshkumar Sundaramoorthy, Srikanth Balijapelly, Sudip Mohapatra, Sutapa Bhattacharya, Kartik Ghosh, and Amitava Choudhury*

Cite This: *Inorg. Chem.* 2024, 63, 11628−11638

Read Online

ACCESS | Metrics & More | Article Recommendations | Supporting Information

ABSTRACT: A series of quaternary selenides, Na_xMGaSe_4 (M = Mn, Fe, and mixed Zn/Fe), have been synthesized for the first time employing a high-temperature solid-state synthesis route through stochiometric or polychalcogenide flux reactions. Along with the selenides, a previously reported sulfide analogue, Na_xFeGaS_4, is also revisited with new findings. These compounds form an interpenetrated structure made up of a supertetrahedral unit. The electrochemical evaluations exhibit a reversible (de)intercalation of ∼0.6 and ∼0.45 Na-ions, respectively, from $Na_{2.87}FeGaS_4$ (**1a**) and $Na_{2.5}FeGaSe_4$ (**2**) involving Fe^{2+}/Fe^{3+} redox when cycled between 1.5 and 2.5 V. Mössbauer spectroscopy of **1a** shows the existence of a mixed oxidation state of $Fe^{2+/3+}$ in the pristine compound and reversible oxidation of Fe^{2+} to Fe^{3+} during the electrochemical cycles. $Na_{2.79}Zn_{0.6}Fe_{0.4}GaSe_4$ possesses a reasonably high room temperature ionic conductivity of 0.077 ms/cm with an activation energy of 0.30 eV. The preliminary magnetic measurements show a bifurcation of FC-ZFC at 4.5 and 2.5 K, respectively, for **1a** and $Na_3MnGaSe_4$ (**4**) arising most likely from a spin-glass like transition. The high negative values of the Weiss constants −368.15 and −308.43 K for **1a** and **4**, respectively, indicate strong antiferromagnetic interactions between the magnetic ions and also emphasize the presence of a high degree of magnetic frustration in these compounds.

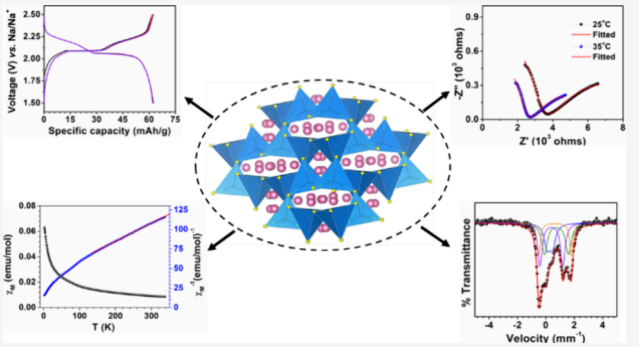

INTRODUCTION

Main-group chalcometallate building units are bestowed with exceptional variety of structural diversity.[1,2] When combined with another main-group metal of different chemical identity or transition metal (d or f-block), a new set of exotic structures can be obtained endowed with fascinating properties, for example, the discovery of crystalline long-range ordered nanotubular phases of $SbPS_{4-x}Se_x$ ($0 \leq x \leq 3$)[3] and Na_xEuTtQ_4 (Tt = Si, Ge, x = 1.5−2)[4,5] through the joining of main-group tetrahedral building-blocks or formation of nanotubes through the joining of a supertetrahedral cluster showing orientation-dependent photoconductivity.[6] The presence of unpaired spins of transition metals in these building units can offer unique electronic and magnetic phenomena. Thus, chalcogenides often offer the real possibility of discovering magnetic semiconductors.[7−9] Often these chalcometallate building units are such that they are of interest by virtue of their structural features. The suitable placement of transition metal ions on them and their corresponding interactions can give rise to quantum materials.[10] One such building unit is the supertetrahedral building unit, in which the presence of unpaired spins at the corners of the supertetrahedron makes them excellent candidates for geometrical magnetic frustration[11] and associated quantum phenomena such as quantum spin liquid.[12−16] Earlier we reported a series of such unpaired spin containing supertetrahedral building units forming interpenetrating zincblende lattices.[17] These materials are highly magnetically frustrated and represent a rich source of a unique frustrated system with a tetrahedral (Td) magnetic lattice. In the chalcogenide family, a frustrated system with a tetrahedral lattice is not common.[18] Recently, we also reported interpenetrating zincblende lattices with Zn-containing T2 units, Na_3ZnGaQ_4, isostructural to the magnetic analogues, Na_3MGaS_4 (M = Mn, Fe, Co), displaying high Na-ion conduction.[19] Following our report, Han et al. substantially improved the Na-ion conductivity in $Na_{3-x}Zn_{1-x}Ga_{1+x}S_4$ by creating a Na-vacancy through an increase in the amount of Ga^{3+} in the structure.[20] With this finding, it was clear that the

Received: March 5, 2024
Revised: May 29, 2024
Accepted: May 30, 2024
Published: June 12, 2024

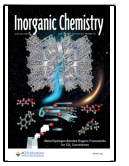

https://doi.org/10.1021/acs.inorgchem.4c00927
Inorg. Chem. 2024, 63, 11628−11638

Table 1. Crystal Data and Refinement Parameters for 1-rev and 1a−1c

Empirical formula	$Na_{2.57}FeGaS_4$ (1-rev)	$Na_{2.87}FeGaS_4$ (1a)	$Na_{2.63}Fe_{0.88}Ga_{1.12}S_4$ (1b)	$Na_{2.66}Fe_{0.86}Ga_{1.14}S_4$ (1c)
Formula weight	312.89	319.79	315.94	316.91
Temperature	293(2) K	298(2) K	299(2)K	223(2)K
Wavelength	0.71073 Å	0.71073 Å	0.71073 Å	0.71073 Å
Crystal system	Tetragonal	Tetragonal	Tetragonal	Tetragonal
Space group	$I4_1/acd$	$I4_1/acd$	$I4_1/acd$	$I4_1/acd$
a/Å	12.964(2)	13.049(2)	12.894(2)	12.859(2)
b/Å	12.964(2)	13.049(2)	12.894(2)	12.859(2)
c/Å	18.792(4)	18.750(3)	18.621(3)	18.582(3)
Volume/Å^3	3158.2(2)	3192.8(2)	3096.1(2)	3072.62(2)
Z	16	16	16	16
Density (calculated)	2.632 Mg/m^3	2.661 Mg/m^3	2.711 Mg/m^3	2.740 Mg/m^3
Absorption coefficient	6.341 mm^{-1}	6.290 mm^{-1}	6.665 mm^{-1}	6.750 mm^{-1}
Goodness-of-fit on F2	1.088	1.175	1.041	1.203
R [$I > 2\sigma(I)$]	R_1 = 0.0276	R_1 = 0.0238	R_1 = 0.0355	R_1 = 0.0151
wR ($F2$) (all data)	wR_2 = 0.0653	wR_2 = 0.0698	wR_2 = 0.0830	wR_2 = 0.0327
Largest diff. peak and hole (e·Å^{-3})	0.552 and −0.379	0.701 and −0.720	0.739 and −0.842	0.340 and −0.407

M/Ga ratio can be varied beyond 1:1 in the mixed-occupancy site by adjusting the amount of Na in the structure. These results have opened up the opportunity to evaluate whether the magnetic lattices can be redox-active with respect to Na-deintercalation in a Na-ion battery as the charge of framework can be balanced through the oxidation of M^{2+} to M^{3+} in Na_3MGaQ_4. Similarly, what happens to Na-ion conductivity if we create a Na-deficiency in the Zn-analogue, $Na_3ZnGaSe_4$ by introducing a +3 ion such as Fe^{3+}? Indeed, our studies have found that electrochemical Na-deintercalation from these lattices is possible with the oxidation of Fe^{2+} to Fe^{3+}. In this article, we have expanded the family of magnetically frustrated lattices to selenide analogues, Na_xMGaQ_4 (M = Mn, Fe, and mixed Zn/Fe) and reported preliminary magnetic data displaying frustration. We have demonstrated that Na-intercalation and deintercalation are topotactic and reversible for the iron-containing phases, Na_xFeGaQ_4 (Q = S, Se). We have also revisited the composition of Na_3FeGaS_4, which can now be more accurately described as Na_xFeGaS_4 (x = 2.57) with a mixed valency of Fe as confirmed by Mössbauer spectroscopy. In this manuscript, we also report a reasonably high ionic conductivity for the mixed Zn/Fe phase.

EXPERIMENTAL SECTION

Materials. Elemental Se, Ga, Mn, Fe, and Zn employed in this work were purchased from Sigma-Aldrich Chemical Co. and used as obtained. Na_2S was purchased from Fisher Scientific. Na_2Se_2 was prepared in a laboratory by mixing stoichiometric quantities of metallic Na and Se in liquid ammonia in a flask in a N_2 environment similar to the reported procedure.[21]

Synthesis of $Na_xFe_yGa_{(1-y)}S_4$ (1a, 1b, 1c), $Na_{2.5}FeGaSe_4$ (2), $Na_{2.79}Fe_{0.4}Zn_{0.6}GaSe_4$ (3), and $Na_3MnGaSe_4$ (4). Different compositional variants of the compound, $Na_xFe_yGa_{(1-y)}S_4$, were synthesized through three different routes. First, we employed our previously reported protocol where a stoichiometric combination of Fe, Ga, S, and Na_2S targeting a nominal composition of Na_3FeGaS_4 was heated in a sealed quartz tube at 750 °C for 96 h (compound **1a**).[17] Two other methods, namely, stoichiometric mixing of elements (compound **1b**) and metathesis routes (compound **1c**) targeting nominal composition of Na_3FeGaS_4, were also employed. In the stoichiometric elemental route, freshly cut metallic Na pieces, Ga shavings, and Fe and S powders in a 3:1:1:4 ratio were loaded in a carbon-coated fused silica ampule and heated to 750 °C for 96 h. On the other hand, for the metathesis route (Na_5GaS_4 + $FeCl_2$ = Na_3FeGaS_4 + 2NaCl), first Na_5GaS_4 was synthesized following our previously reported procedure.[22] Then in the second step, thoroughly mixed Na_5GaS_4 and $FeCl_2$ in a 1:1 ratio were loaded in the carbon-coated fused silica tube inside an Ar-filled glovebox, vacuum sealed, and heated to 750 °C for 48 h with a heating and cooling rate of 25 °C/h. The compounds $Na_{2.5}FeGaSe_4$ (**2**) and $Na_{2.79}Fe_{0.4}Zn_{0.6}GaSe_4$ (**3**) were synthesized by the stochiometric combination of elements. For **2**, 3 mmol Na, 1 mmol Fe, 1 mmol Ga, and 4 mmol Se were taken. For **3**, in place of 1 mmol Fe, a mixture of Fe and Zn was taken in 0.5 mmol quantities of each with other reactants remaining the same as in **2**. All the precursors were weighed according to the above-mentioned stoichiometric ratio and loaded into a carbon coated quartz ampule inside an argon filled glovebox. The ampules were attached to the adaptors before being taken out of the glovebox to avoid exposure to air and moisture and subsequently flame-sealed under vacuum. The sealed ampules were heated to 750 °C for 120 h and then cooled with a heating and cooling ramp of 20 °C/h and 35 °C/h, respectively. Dark red to completely dark crystals of compounds **1a, 1b, 1c, 2,** and **3** were obtained after breaking the ampules inside the glovebox. The compound, $Na_3MnGaSe_4$ (**4**), on the other hand, was synthesized using Na_2Se_2 flux along with elemental Mn, Ga, and Se. In a nitrogen filled glovebox (O_2 < 1 ppm), 1 mmol Mn, 1 mmol Ga, 2.5 mmol Se, and 3 mmol Na_2Se_2 were loaded into a quartz ampule that was flame-sealed under vacuum and placed in a furnace. The temperature was increased from 25 to 700 °C at a rate of 20 °C/h, kept at 700 °C for 96 h, and then cooled to room temperature at a rate of 20 °C/h rate. The product was washed with *N,N*-dimethylformamide to remove excess polychalcogenide flux and byproducts. The dark red color slightly moisture sensitive product consisting of chunks of crystals was obtained after washing. Suitable crystals obtained from the as synthesized or DMF-washed samples were chosen under an optical microscope and used for the single crystal X-ray diffraction.

X-ray Crystallography. Good quality single crystals were chosen under an optical microscope and mounted on a glass fiber for single-crystal X-ray diffraction. A Bruker Smart Apex II diffractometer with monochromated Mo Kα radiation (λ = 0.7107 Å) was used to collect the data. The data sets were collected at various temperatures between 200 and 293 K using Smart or Apex II software with a step of 0.3° in a ω scan and 20 s/frame exposure time. The data integration and absorption corrections were carried out through SAINT[23] and SADABS[23] programs, respectively. The crystal structures were solved by SHELXS-97 and difference Fourier syntheses. Full-matrix least-squares refinement against $|F^2|$ was carried out using the SHELXTL-PLUS suite of programs.[24] All of the compounds crystallized in the $I4_1/acd$ space group, similar to our previously reported isostructural compounds. The asymmetric unit consisting of two sodium atoms, one gallium atom, and three chalcogen atoms was located from the Fourier maps. The initial isotropic refinement showed the absence of

https://doi.org/10.1021/acs.inorgchem.4c00927
Inorg. Chem. 2024, 63, 11628−11638

further electron densities and reasonable thermal parameters. However, the weighted R factor, wR_2, did not converge to a lower value, suggesting the possibility of mixed occupancy in the gallium site (Ga/M). Therefore, the Ga site was freely refined with mixed Ga and M (Fe, Mn, and Fe/Zn) occupancy, which significantly reduced the weighted R factor. For the mixed metal Ga/Zn/Fe, occupancy of all three (Ga, Zn, and Fe) atoms was freely refined using the SUMP instruction. In all cases, the overall occupancy was constrained to 100%, keeping their coordinates and atomic displacement parameters (ADPs) same. Such constraint led to a 50:50 occupancy for M and Ga for **1a**, **2**, and **4**, but **1b** and **1c** showed deviations from a 1:1 ratio of Fe:Ga. However, for **3**, such refinements yielded occupancies of Ga1, Zn1, and Fe1 to be 0.51 (2), 0.31 (2), and 0.18 (2), which for final refinement was constrained to be 50, 30, and 20%.

Finally, for the Fe-containing phases, out of the two Na-ions, one (Na2) showed higher ADP and an unaccounted-for e-density (1.2 e/Å^3) close to it. The occupancy of the Na2 site was refined freely along with a split position of Na2 (Na2A). All of the Fe-containing phases showed partial occupancy in Na2 split sites, and such refinements improved the R-factors for all of them. In the final stages of refinements, the occupancy of Na1 was also varied and found to be very close to the full occupancy or slightly underoccupied. No such underoccupancy was found for the Mn-selenide phase (**4**). Realizing the prevalence of underoccupancy in the Na-site in the Fe-containing phases, it prompted us to revisit our earlier published compound, Na_3FeGaS_4,[17] and we found two unfortunate errors in the previous solution. The diffraction data set was mistakenly refined with low temperature unit cell parameters, whereas the data set was collected under dry N_2 purging at room temperature, and also, occupancies of Na positions were not refined. In this article, we are correcting those errors with new refinement of the old data sets yielding a slightly bigger unit cell and a revised composition, $Na_{2.57}FeGaS_4$ (**1-rev**). The final compositions from crystallographic refinements are as follows: $Na_{2.57}FeGaS_4$ (**1-rev**), $Na_{2.87}FeGaS_4$ (**1a**), $Na_{2.63}Fe_{0.88}Ga_{1.12}S_4$ (**1b**), $Na_{2.66}Fe_{0.86}Ga_{1.14}S_4$ (**1c**), $Na_{2.5}FeGaSe_4$ (**2**), $Na_{2.79}Fe_{0.4}Zn_{0.6}GaSe_4$ (**3**), and $Na_3MnGaSe_4$ (**4**). The charge-balance for the Na-deficient phases has been accomplished via the oxidation of Fe^{2+} to Fe^{3+} leading to mixed valency in those compounds as proved in the case of **1a**−**1c** from Mössbauer spectroscopy (discussed later). The final anisotropic refinements on all compounds were performed via SHELX-2014 incorporated in ShelXLe.[25] The crystal data and final refinement parameters for **1-rev, 1a**−**1c**, and **2**−**4** are given in Tables 1 and 2, and important interatomic distances are given in Tables 3 and 4. The atomic coordinates are supplied in the Supporting Information (Table S1). Finally, the bulk purity of the compounds was evaluated by using laboratory powder X-ray diffraction data.

Powder X-ray Diffraction. To evaluate the bulk purity of all the compounds, laboratory powder X-ray diffraction patterns were collected from a PANalytical X'Pert Pro diffractometer equipped with a Cu Kα anode and a linear array PIXcel detector over a 2θ range of 5 to 90° with a scan rate of 0.0472° s^{-1}. The compounds were hand ground using a mortar and pestle into fine particles inside an Ar-filled glovebox and loaded into an airtight sample holder with a Kapton film window to collect the diffraction patterns. The collected experimental PXRD patterns are a good match with our simulated powder patterns obtained from single-crystal X-ray diffraction, confirming the bulk purity of the compounds except for **1a**−**1c** (Figures S1a and S1b). In the case of compounds **1a**−**1c**, the presence of varying amounts of the major impurity phase, $Na_3Fe_2S_4$,[26] can be observed. The amount of impurity was quantified employing Mössbauer spectroscopy (discussed below). On the other hand, for compounds **2** and **3**, a slight Na-deficiency should result in minor impurities. After close inspection and taking a cue from the sulfide phase, some low intense impurity lines can be attributed to the $Na_3Fe_2Se_4$ phase.[27]

Electrochemical Characterization. The electrode preparation and battery fabrication were carried out inside an Ar-filled glovebox with O_2 < 0.2 ppm and H_2O < 0.2 ppm. The active materials (compounds **1a** and **2**) were mixed with conducting carbon (super-P) and poly(vinylidene fluoride) in a ratio of 75:15:10 by hand grinding for 30 min with a mortar and pestle. The cathode slurry was made by dispersing the well-ground samples with N-methyl-2-pyrrolidone (NMP) and coating them on aluminum foil. The cathode was prepared by heating the slurry under vacuum at 80 °C for 12 h. CR2032 type coin cells were assembled with Na as the anode, 1 M $NaClO_4$ dissolved in EC:DMC as the electrolyte, and Whatman glass fiber as separator. All galvanostatic tests were carried out in a NEWARE BT-4000 battery cycler. Cyclic Voltammetry (CV) was performed using a PAR EG&G potentiostat/galvanostat model with a scan rate of 0.05 mV/s. All the electrochemical tests were conducted between a potential range of 1.5 and 2.5/3.0 V for compound **1a** and 1.5 to 2.1 V for compound **2** unless otherwise mentioned. To examine the maximum limit of Na intercalation into the structure and analyze the polarization, the Galvanostatic Intermittent Titration Technique (GITT) was performed on compound **1a** at 10 mA/g current density with a current pulse for 60 min followed by a relaxation time of either 120 or 240 min. To perform the post cycle analysis (PXRD and Mössbauer) of the cathodes, the cells were charged or discharged to the required potential in constant current (CC) mode. Once the desired potential is reached, constant voltage mode charge or discharge of the cells was performed for 1 h to equilibrate the cell

Table 2. Crystal Data and Refinement Parameters for 2−4

Empirical formula	$Na_{2.5}FeGaSe_4$ (**2**)	$Na_{2.79}Fe_{0.4}Zn_{0.6}GaSe_4$ (**3**)	$Na_3MnGaSe_4$ (**4**)
Formula weight	498.83	511.26	509.47
Temperature	296(2) K	200(2) K	293(2) K
Wavelength	0.71073 Å	0.71073 Å	0.71073 Å
Crystal system	Tetragonal	Tetragonal	Tetragonal
Space group	$I4_1/acd$	$I4_1/acd$	$I4_1/acd$
a/Å	13.349(4)	13.437(2)	13.758(8)
b/Å	13.349(4)	13.437(2)	13.758(8)
c/Å	19.392(6)	19.271(3)	19.571(5)
Volume/ Å^3	3456.0(2)	3479.7(6)	3704.0(5)
Z	16	16	16
Density (calculated)	3.835 Mg/m^3	3.904 Mg/m^3	3.654 Mg/m^3
Absorption coefficient	21.678 mm^{-1}	22.198 mm^{-1}	20.045 mm^{-1}
Goodness-of-fit on F2	1.086	1.08	1.095
R [$I > 2\sigma(I)$]	R_1 = 0.0363	R_1 = 0.0214	R_1 = 0.0225
wR ($F2$) (all data)	wR_2 = 0.0761	wR_2 = 0.0554	wR_2 = 0.0579
Largest diff. peak and hole (e·Å^{-3})	0.842 and −0.793	0.631 and −0.853	0.552 and −0.534

Table 3. Selected Bond Lengths (Å) for $Na_xFe_yGa_{(1-y)}S_4$ (1-rev, 1a−1b)

Moiety	1-rev	1a	1b	1c
Ga1/M1 − S1	2.3039(9)	2.3197(7)	2.2829 (8)	2.2789 (6)
Ga1/M1 − S1[a]	2.3200(9)	2.3373(7)	2.2983 (9)	2.2947 (6)
Ga1/M1 − S2	2.3334(7)	2.3491(5)	2.3126(8)	2.3092(4)
Ga1/M1 − S3	2.3690(8)	2.3919(6)	2.3439(9)	2.3387(5)

[a]Symmetry operation: $-y + 3/4, x - 1/4, -z + 1/4$.

Table 4. Selected Bond Lengths (Å) for Na_xMGaSe_4 (2−4)

Moiety	2	3	4
Ga1/M1 − Se1	2.389(2)	2.3931(6)	2.459(2)
Ga1/M1 − Se1[a]	2.404(2)	2.4125(6)	2.477(2)
Ga1/M1 − Se2	2.419(2)	2.4287(5)	2.489(2)
Ga1/M1 − Se3	2.446(2)	2.4618(6)	2.533(2)

[a]Symmetry operation: $-y + 3/4, x - 1/4, -z + 1/4$.

https://doi.org/10.1021/acs.inorgchem.4c00927
Inorg. Chem. 2024, 63, 11628−11638

voltage and reduce the IR drop before disassembling the cells and recovering the cathode for further analysis.

Mössbauer Spectroscopy. ^{57}Fe Mössbauer spectroscopy was carried out on as-prepared samples (**1a**, **1b**, and **1c**) as well as electrochemically charged (2.5 V) and discharged (1.5 V) samples for **1a** in transmission geometry using a constant acceleration spectrometer equipped with a ^{57}Co (10 mCi) gamma source embedded in a Rh matrix. The samples were loaded inside the glovebox on a one-centimeter hole of a square shaped (2 × 2 cm^2) lead strip (sample holder), and the sample holders were heat sealed with Kapton film to avoid contact with the air. The instrument was calibrated for velocity, and isomer shifts are reported with respect to α-Fe foil at room temperature. The resulting Mössbauer data were analyzed using Lorentzian profile fitting by RECOIL software.[28]

AC Impedance Measurements. AC impedance measurements were performed from 1 Hz to 1 MHz using a Biologic Instruments SP-150 impedance analyzer with an AC signal amplitude of 100 mV. The hand ground samples were cold pressed by applying a force of 280 MPa in a stainless-steel pressing die inside an argon filled glovebox (O_2 < 0.2 ppm). Indium foil, which acts as a blocking electrode, was used on both sides of the pellet and placed in an airtight Swagelok type cell holder to measure the temperature dependence of ionic conductivity in a temperature-controlled box furnace. The impedance data were collected at every 10 °C increment by keeping the temperature of each measurement constant for at least an hour to reach thermal equilibrium.

Magnetic Measurements. A Quantum Design MPMS SQUID magnetometer was employed to measure the molar magnetic susceptibility of **1a** and **4** while warming from 2 to 300 K in a 2 T applied field under zero-field and field-cooled (ZFC and FC) conditions. The isothermal magnetization measurements were conducted in an applied magnetic field of 0 to 5 T for **1a** and −5 to +5 T for **4** at 5 and 4.27 K, respectively.

RESULTS AND DISCUSSION

Crystal Structure Description and Mixed Valency. The compounds, **1-rev**, **1a-1c**, and **2**−**4**, crystallize in the $I4_1/acd$ space group. The asymmetric units as given in Figure 1 contain

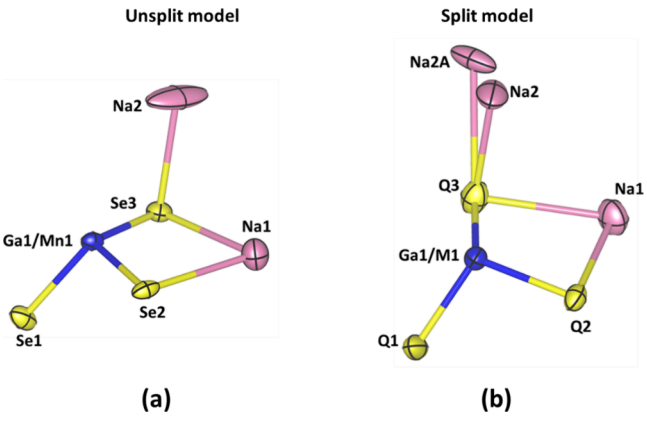

Figure 1. Asymmetric unit of Na_xMGaQ_4 with thermal ellipsoids given at 40% probability showing the unsplit Na-site (a) and split Na-site (b) models.

two sodium atoms, three chalcogen atoms (Q = S or Se), and one site with mixed occupancy of Ga/*M* (*M* = Fe and Mn) or mixed with three elements (Ga, Zn, and Fe for **3**). The compounds **1-rev**, **1a**, and **2**−**4** have equal occupancy of M and Ga, while for **1b** and **1c**, the ratios of Fe and Ga are 0.88:1.12 and 0.86:1.14, respectively. One Na atom (Na1) and a second one with its split positions (Na2, Na2a), one chalcogen atom (Q1), and Ga/*M* sites all occupy the 32*g* Wyckoff site. Q2, Q3, and Na1 occupy 16*e*, 16*b*, and 16*c* positions, respectively. In the case of compound **3**, Fe, Zn, and Ga occupy the same 32*g* site. Note that for **4** we did not find any Na-disorder and the Na2 site is modeled as an unsplit unique position. The chemical formula is represented by doubling the asymmetric unit, and the unit cell contains 16 such units.

The crystal structure of this structure type has been comprehensively discussed in two of our previous publications for different compositions.[17,19] Here, we briefly touch upon the main features of the crystal structure. Four Ga/*M*-centered tetrahedra form a supertetrahedral T2 unit, such T2 units are corner-shared to form a diamond lattice, and two such diamond lattices are interlocked as shown in Figure 2a-e. The extraframework Na-ions fill the channels formed by the two interpenetrating diamond lattices. The Na-ions (Na1 and Na2/Na2a) adopt very distorted octahedral coordination surrounded by 6 chalcogen atoms (Figure S2). The Ga(1)/*M* (1)−Q distances are also in agreement with the identity of the metal and their oxidation state. For example, the average Ga1/$Fe^{2+/3+}$−Se distance in **2** is much smaller (2.415 (2) Å) compared to the average Ga1/Mn^{2+}−Se distance (2.489 (2) Å) as the ionic radii of Fe^{2+} (0.63 Å in Td) and Fe^{3+} (0.49 Å in Td) are smaller than Mn^{2+} (0.66 Å in Td). Ga/Mn−Se bond distances range from 2.459 (2) to 2.533 (2) Å and are at the median of the reported pure Ga−Se and Mn−Se bond lengths as in $NaGa_3Se_5$[29] and $Na_2Mn_2Se_3$,[30] which are in the range 2.347 (2)−2.481 (3) Å and 2.520 (2)−2.603 (3) Å, respectively. However, such a comparison is not appropriate for the Fe-containing phases (**1-rev**, **1a**− **1c**, **2**, and **3**) due to the presence of mixed valency in Fe, and on top of that, there is another metal (Ga/$Fe^{2+/3+}$/Zn^{2+}) substitution in **3**. However, with the Fe-sulfide series (**1-rev**, **1a**−**1c**), there is a consistent decrease of Ga/Fe−S distances as a function of increasing the Fe^{3+} percentage (Table 3).

As mentioned earlier that even after employing three different routes of reactions we were unsuccessful in synthesizing the pure phase of fully stoichiometric Na_3FeGaS_4 or Na_xFeGaS_4, varying amounts of $Na_3Fe_2S_4$ impurity were always present as revealed by the PXRD of the as-synthesized materials (Figure S1). To quantify the impurity phase and determine the ratio of Fe^{2+}/Fe^{3+} in $Na_xFe_yGa_{(1-y)}S_4$, Mössbauer spectra were collected from samples of three different synthesis routes and given in Figure S3 for **1a**−**1c**. The fitted parameters based on Lorentzian site analysis, especially isomer shift (IS), quadrupole splitting (QS) values, and site populations, are given in Table S2. The fitting of the data was challenging due to the presence of an impurity phase, $Na_3Fe_2S_4$, which is also a mixed valent compound. However, fortunately $Na_3Fe_2S_4$ displays one doublet (IS = 0.34 (4), QS = 1.73 (2) mm s^{-1}) due to the rapid valence fluctuation in the Mössbauer time scale representing an average valence state.[31] Therefore, the Mössbauer spectra of compounds **1a**−**1c** are fitted with four doublets as shown in Figure S2a, b, and c, and the site analysis clearly shows the existence of a mixed oxidation state of Fe at the tetrahedral site. The IS values in the range 0.23 (5)−0.28 (5) and QS values of 0.35 (3)−0.41 (2) mm s^{-1} for doublet-1 have been assigned to Fe^{3+}, while two doublets, #2: IS in the range 0.66 (3)−0.70 (3) and QS values of 2.18 (3)−2.27 (4) mm s^{-1} and #3: IS in the range 0.64 (2)−0.74 (2) and QS values of 1.48 (2)−1.75 (3) mm s^{-1}, have been assigned to Fe^{2+} of **1a**, **1b**, and **1c** (see Table S2). Though there is only one crystallographically distinct Fe-atom,

https://doi.org/10.1021/acs.inorgchem.4c00927
Inorg. Chem. 2024, 63, 11628−11638

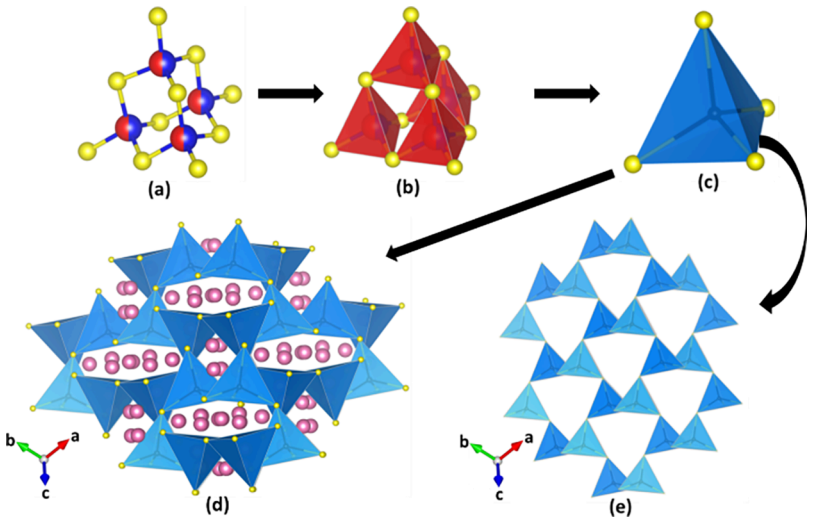

Figure 2. Crystal structure of Na_xMGaQ_4 showing the building up of the 3-dimensional network from supertetrahedral T2 units. (a) Ball-and-stick model of the T2 unit. (b) polyhedral view of the T2 unit. (c) supertetrahedra are represented by a single tetrahedron with a dummy atom at the centers. (d) Diamond lattice made up of a T2 unit filled with Na-ions. (e) Interpenetrating diamond lattices.

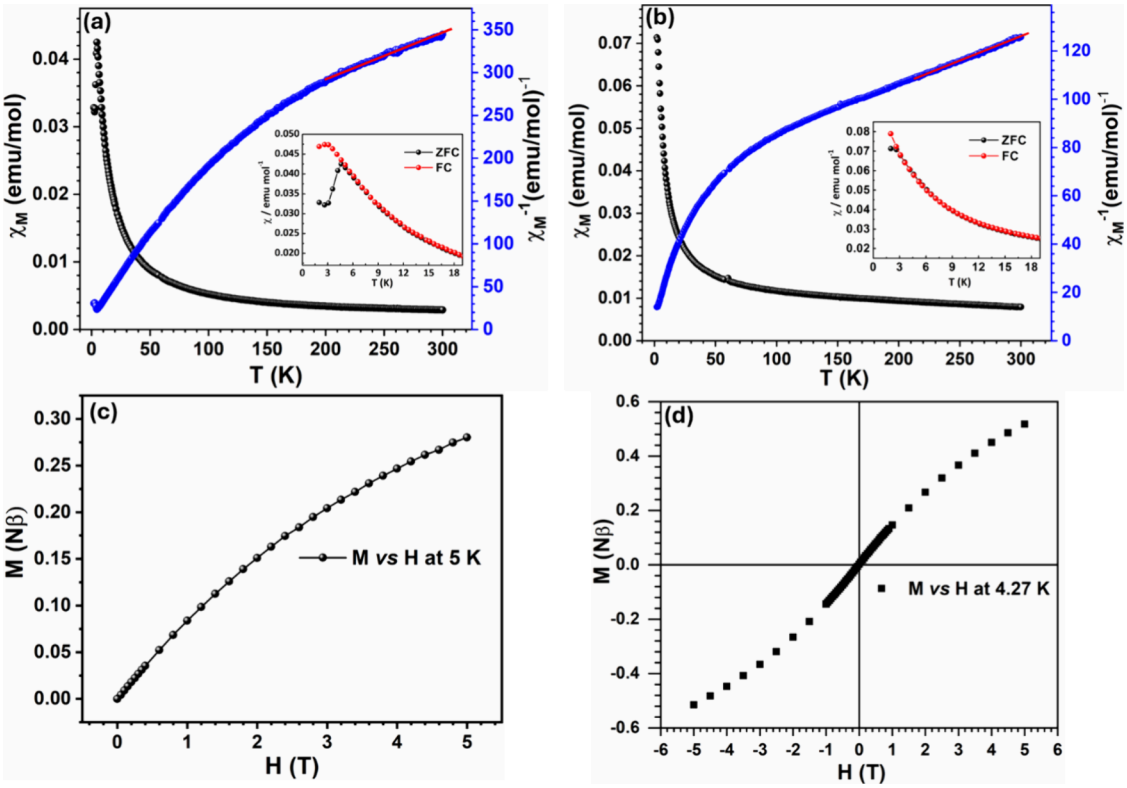

Figure 3. Temperature dependent molar magnetic susceptibility (χ_M) and inverse molar magnetic susceptibility (χ_M^{-1}) at a 2 T applied magnetic field for (a) $Na_{2.87}FeGaS_4$ (**1a**) and (b) Na_3MnGaS_4 (**4**). The inset shows ZFC-FC divergence at lower temperature. (c) Magnetization (M) vs field (H) plot of **1a** and (d) magnetization vs field variation for a hysteresis plot of **4**.

the widths of the doublets are broad due to the disorder from mixed occupancy (Ga/Fe) as well as the presence of Fe^{2+}/Fe^{3+} in the same site and the possible presence of varying degrees of Fe^{2+}/Fe^{3+} in the same sample. Thus, the Fe^{2+} site is fitted with two doublets which can be reported as the weighted-average values of IS and QS, $\langle\delta\rangle_a$ = 0.66 (2) and $\langle\Delta E_Q\rangle_a$ = 1.96 (2) mm s^{-1}, $\langle\delta\rangle_a$ = 0.65 (2) and $\langle\Delta E_Q\rangle_a$ = 1.87 (2) mm s^{-1}, and $\langle\delta\rangle_a$ = 0.71 (2) and $\langle\Delta E_Q\rangle_a$ = 2.07 (2) mm s^{-1} for **1a**, **1b**, and **1c**, respectively. The IS and QS values are in agreement with the reported values of Fe^{2+} and Fe^{3+} in the tetrahedral sulfide environment.[32,33] The ratio of site populations of Fe^{2+} and Fe^{3+} in **1a**, **1b**, and **1c** can now be derived by taking into account the percentage of the impurity phase ($Na_3Fe_2S_4$), which is ~38, 15.5, and 43%, respectively, and normalizing the remaining Fe^{2+} and Fe^{3+} to 100%. Thus, approximately ~87, 72, and 59.5% of Fe in the 2+ oxidation state and the remaining percentage of Fe in the 3+ oxidation state, respectively, can be found for the three routes of synthesis

https://doi.org/10.1021/acs.inorgchem.4c00927
Inorg. Chem. 2024, 63, 11628−11638

Table 5. Curie–Weiss Fitting Parameters, Experimental and Theoretical μ_{eff}, Frustration Index, Maximum Experimental Magnetization Achieved at 5 T, and Theoretical Saturated Magnetization for 1a and 4

Compd	C (emuK/mol)	Θp (K)	μ_{eff} (exp.)	μ_{eff} (theo.)[a]	f = IΘpI/T*	M (Nβ)[b]	M_s(Nβ)$_{max}$[c]
1a	1.935	−368.15	3.93	5.29	81.81	0.280	4
4	4.743	−308.43	6.16	5.91	154.21	0.517	5

[a]Spin-only theoretical μ_{eff}. [b]Experimental Magnetization achieved at 5 T. [c]Theoretical Saturated Magnetization.

from which **1a**, **1b**, and **1c** are obtained. The Fe2+ and Fe3+ percentages match (indirectly from Na-occupancy refinement) with the crystallographically derived composition for **1a**, $Na_{2.87}Fe^{2+}_{0.87}Fe^{3+}_{0.13}GaS_4$ (87% Fe^{2+}), and **1b**, $Na_{2.63}Fe^{2+}_{0.63}Fe^{3+}_{0.25}GaS_4$ (71.5% Fe^{2+}), but deviate significantly for the metathesis route, **1c**, $Na_{2.63}Fe^{2+}_{0.63}Fe^{3+}_{0.23}GaS_4$ (crystallography-Fe^{2+} = 73.3% vs Mossbauer-Fe^{2+} = 59.5%). These values indicate that even in the same synthesis, the ratio of Fe^{2+}/Fe^{3+} can vary, and Mössbauer data should be used to determine the redox properties of the bulk rather than the crystallographic composition from one single-crystal.

Magnetic Properties. In this work, the temperature dependent-zero-field-cooled dc magnetic measurements of the polycrystalline sample of compound **4** are reported for the first-time using SQUID MPMS. We have also revisited the magnetic properties of compound **1a**. The temperature dependent molar susceptibility (χ_M) and inverse molar magnetic susceptibility ($1/\chi_M$) of compounds **1a** and **4** at an applied field of 2 T from 2 K to room temperature are shown in Figure 3. The molar magnetic susceptibility of the compounds increases asymptotically while lowering the temperature and reaches the maximum values of 0.043 and 0.071 emu mol^{-1} for compounds **1a** and **4** at temperatures of 4.5 and 2.5 K, respectively. After 4.5 K, there is a sharp fall in χ_M in the ZFC data for **1**, while the FC data continue to rise showing a bifurcation (inset Figure 3a). Such a bifurcation of FC-ZFC data often represents a signature of spin glass like transition.[12,34,35] In the case of compound **4**, after 2.5 K, the χ_M value becomes constant for the ZFC, while FC data keeps increasing, showing a divergence reminiscent of spin glass transition (inset of Figure 3b). The $1/\chi_M$ vs T plot shows linearity in the temperature range of 200–300 K and 150–300 K for compounds **1a** and **4**, respectively, indicating paramagnetic regions; below those temperature ranges the plots tend to deviate from the linearity. The linear fitting of the data in the paramagnetic region with Curie–Weiss law ($1/\chi_M = (T - \theta_p)/C$) provides the Curie constant, C, and Weiss constant, θ_p, as listed in Table 5.

The large negative θ_p (−368.15 and −308.43 K for **1a** and **4**, respectively) indicates the presence of strong antiferromagnetic interactions between the adjacent transition metal centers with a high degree of magnetic frustration.[11] The effective magnetic moments (μ_{eff}) for the compounds as calculated from the Curie constant, C, are compared with the theoretical spin-only magnetic moment as listed in Table 5. The experimental μ_{eff} of compound **1a** (3.93 μ_B) is significantly lower than the theoretical μ_{eff} value of 5.03 μ_B assuming a spin-only moment of 87% Fe^{2+} and 13% Fe^{3+}. Such a significant difference in the μ_{eff} may arise due to substantial antiferromagnetic interactions in the selected linear fit region, which means instead of a purely paramagnetic interaction, the fitted region was riding on some kind of short-range ordering. One can also notice a curvature-like behavior in the $1/\chi_M$ vs T plot between 50 and 300 K instead of a truly linear one as one would see for a purely paramagnetic region. The presence of a minor $Na_3Fe_2S_4$ impurity cannot be completely ruled out, though hand-picked crystals of pure **1a** were used for measurements. In the case of compound **4**, the calculated μ_{eff} (6.0 μ_B) is slightly higher than the theoretical spin only moment of 5.92 μ_B. The isothermal magnetization measurements of compounds **1a** and **4** at 5 and 4.27 K, respectively, show a sluggish rise in the magnetization with the change in magnetic field (Figures 3c and 3d). Compounds **1a** and **4** reached maximum magnetization values of 0.28 and 0.51 Nβ, respectively, at 5 T which are significantly lower than the theoretical saturation moment of the free ion as calculated from the number of unpaired electrons assuming parallel spins (M_s = gSNβ) as listed in Table 5.

Lower magnetization values along with the absence of any hysteresis while reversing the magnetic field (in case of **4**) validate the presence of strong antiferromagnetic interactions. To understand the nature of magnetic interactions, we refer to the structural T2/supertetrahedral unit (Figure 2a-c), and the antiferromagnetic interactions between the magnetic ions in the tetrahedral unit would lead to magnetic frustration. The magnetic frustration can be measured by the frustration parameter, $f = |\theta_p|/T^* > 10$, where T* is the transition temperature.[11] The frustration index calculated for both compounds, **1a** (368.15/4.5 = 81.81) and **4** (308.43/2.5 = 123.37), is significantly high, supporting the presence of magnetic frustration. Also note that this frustrated system is disordered due to the mixed occupancy (50/50) of the transition metal and Ga in the same crystallographic site. This random frustration system due to dilution in the magnetic site can lead to a spin-glass like ground state as evident by the FC-ZFC divergence.[34,35] In this revisit of **1a**, we observed not only a mixed valency of Fe but also a FC-ZFC divergence, which was not observed in our earlier study.[17] These differences may arise due to the presence of different amounts of impurity phases in the two syntheses, and also the ratio of Fe^{2+} and Fe^{3+} is different. However, it will require more measurements in a low applied field as well as frequency-dependent AC measurements to understand the nature of magnetic transition.

Sodium Ion Electrochemistry. Early works on sulfide-based cathodes for Na-ion intercalation were explored on TiS_2 as the host for Na^+ ions by Whittingham.[36] The host exhibited 0.3 V lower intercalation voltage compared to the $LiTiS_2$ analogue and displayed a complex coordination of Na^+ ions (octahedral and prismatic). Following this report, various chalcogen-based hosts were explored for Na-ion intercalation.[37] Though the sulfide-based materials show low working voltage, a recent spike in literature showing the possibilities of reversible anionic redox in chalcogen cathodes has intrigued researchers to revisit the chalcogen hosts.[38–40] In that spirit, here we report the electrochemical activity of Na_xFeGaQ_4 (Q = S and Se) mainly to investigate if oxidative deintercalation of Na is possible with complete conversion of Fe^{2+} to Fe^{3+}. To the best of our knowledge, this is the first example of a chalcogen-based polyanionic material for Na^+ ion intercalation having structural flexibility for tuning the composition. The theoretical capacities calculated for (de)intercalation of one

https://doi.org/10.1021/acs.inorgchem.4c00927
Inorg. Chem. 2024, 63, 11628–11638

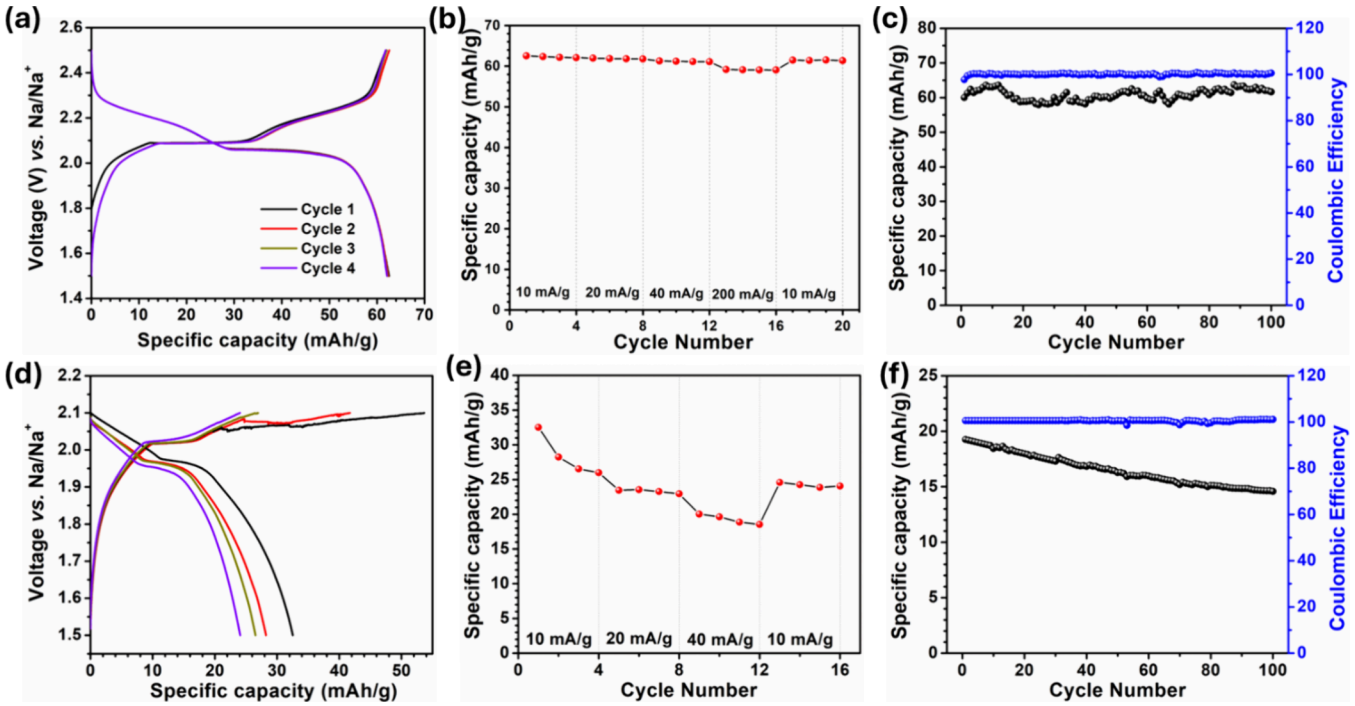

Figure 4. Galvanostatic charge−discharge curves at 10 mA/g current density, capacity retention at different C-rates, and a long cycle test at 40 mA/g current density of $Na_{2.87}FeGaS_4$ (a-c) and $Na_{2.5}FeGaSe_4$ (d-f).

mol Na in compounds **1a** and **2** are 83.80 and 53.72 $mAhg^{-1}$, respectively. However, note that from Mössbauer analysis, the **1a** sample is a mixture of $Na_{2.87}FeGaS_4$ (62%) and $Na_3Fe_2S_4$ (38%), where the impurity phase is also a potential candidate for Na-ion deintercalation. The electrochemical measurements of compound **1a** were carried out first in the potential range of 1.5−2.5 V at a current density of 10 mA/g, and the corresponding charge and discharge curves of the first four cycles are presented in Figure 4a. The plot clearly shows an initial sloppy profile followed by a flat plateau displaying highly reversible electrochemical (de)intercalation achieving ∼63 mAh/g capacity with a very small polarization of ∼35 mV. The dQ/dV plot of compound **1a** shows perfectly reversible redox peaks, a sharp one at ∼2.05 and a broad at ∼2.2 V, for the flat and sloppy profiles, respectively, supporting the involvement of $Fe^{2+/3+}$ couples as shown in Figure S4a. This achieved capacity cannot be explained solely from ∼0.87 Na removal from 62% of **1a** in the cathode mix (83.82 mAh/g × 0.87 × 0.62 = 45.21 mAh/g) indicating that the $Na_3Fe_2S_4$ impurity phase is also electrochemically active (evident from Mössbauer spectra, discussed later). The material also exhibits good reversibility of Na^+ extraction and reinsertion even at high current density of 200 mA/g as shown in Figure 4b with an average potential of 2.08 V. Further, the structure displayed a high degree of stability (Figure S4b, PXRD of the cycled cathode) even after 100 cycles at 40 mA/g current density (Figure 4c), elucidating that this model structure type can be a new platform for the exploration of polyanionic sulfide-based cathode chemistry in Na-ion batteries.

Observing interesting electrochemical activities in the sulfide analogue, we tested its selenide analogue, compound **2**, which also turned out to be electrochemically active. It is expected that compound **2** will have lower potential than its sulfide version due to less electronegativity of Se compared to S as also shown in the previous chalcogen based cathode materials.[41] The cycling was carried out in the potential range of 1.5−2.1 V at 10 mA/g current density, and the initial charge/discharge curves are shown in Figure 4d. Initially ∼1.0 Na^+ ions are extracted from the structure, but on the consecutive cycles only, ∼0.45 Na^+ ions could be reversibly extracted and reinserted. The charging and discharging curves are rather sloppy without any discernible plateaus, indicating a solid solution type behavior of the redox active phase. The cyclic voltammetry of compound **2** showing reversible anodic and cathodic peaks at 2.07 and 1.92 V is a clear indication of the reversible $Fe^{2+/3+}$ redox process during the charge and discharge cycles (Figure S5). However, compound **2** suffers from poor cycle reversibility at high current rates as shown in Figures 4e and 4f. The capacity decays slowly when the battery is subjected to a long cycle life at a 40 mA/g current density. Poor capacity retention of compound **2** may be due to oxidation of the Se^{2-} anion in the initial cycles resulting in structural rearrangement. Although these materials cannot compete with the current Na-ion cathodes in terms of capacity, the structural stability of sulfides and availability of more Na^+ ions in these materials make them excellent model candidates for further exploration of polyanionic-based 3-D chalcogenide especially as a host for dual cation and anion redox candidates and fast charging Na-ion batteries.

Charge Compensation Mechanism. To elucidate the charge compensation of $Fe^{2+/3+}$ redox during the (de)-intercalation of Na^+ ions, we performed *ex situ* ^{57}Fe Mössbauer spectroscopic analyses on a bulk sample of **1a**, its charged and discharged states. To track the changes in oxidation states during charge and discharge, two coin-cells were disassembled, one after the first charge and another after the first discharge, to collect the electrochemically oxidized and reduced samples, respectively, for Mössbauer spectroscopic analysis, and the results are given in Figure 5 and Table 6. The spectrum of the fully charged sample (Figure 5b) can be deconvoluted into two

https://doi.org/10.1021/acs.inorgchem.4c00927
Inorg. Chem. 2024, 63, 11628−11638

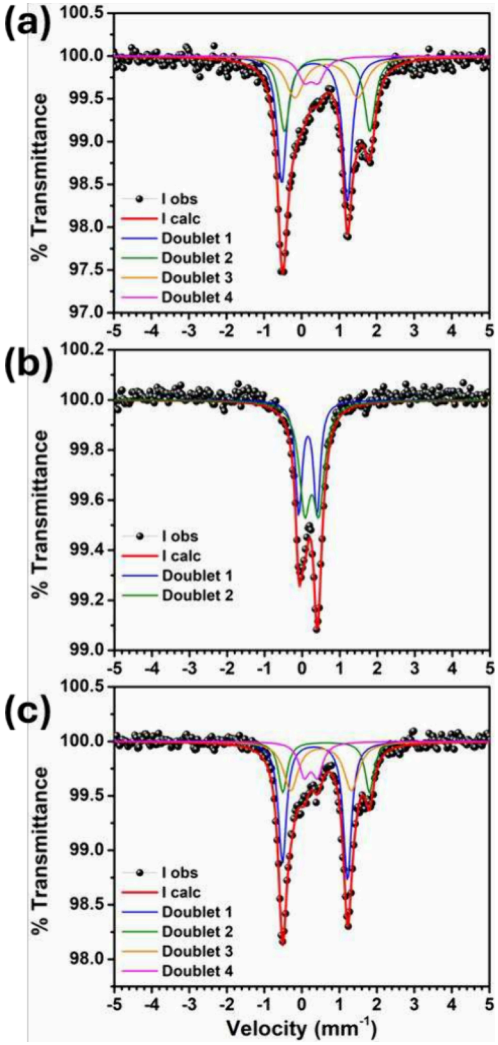

Figure 5. Mössbauer spectra of $Na_{2.87}FeGaS_4$ (a) pristine, (b) fully charged, and (c) fully discharged.

Table 6. Mössbauer Spectroscopic Values for the Isomer Shift (IS) and Quadrupole Splitting (QS) of Pristine, Charged, and Discharged Phases of $Na_{2.87}FeGaS_4$

Compound	Site	IS (δ) (mm s^{-1})	QS (ΔE_Q) (mm s^{-1})	Site population (%)
Na_2S-Stoichiometry	Delocalized Doublet 1	0.34(2)	1.74(3)	38(5)
1a	Fe^{2+}-Doublet 2	0.68(5)	2.27(4)	27(2)
	Fe^{2+}-Doublet 3	0.64(3)	1.64(2)	26(5)
	Fe^{3+} Doublet 4	0.28(5)	0.38(2)	8(3)
Discharged	Delocalized Doublet 1	0.35(4)	1.73(2)	38.8(2)
	Fe^{2+}-Doublet 2	0.65(3)	2.31(8)	17.1(5)
	Fe^{2+}-Doublet 3	0.51(5)	1.60(2)	33.7(3)
	Fe^{3+} Doublet 4	0.25(2)	0.33(3)	10.3(4)
Charged	Fe^{3+}-Doublet 1	0.15(4)	0.48(3)	40(4)
	Fe^{3+}-Doublet 2	0.25(4)	0.37(2)	60(2)

doublets, one with IS and QS values of 0.25 (4) and 0.38 (2) mm s^{-1} with a site population of ~61% and another with 0.15 (4) and 0.48 (3) mm s^{-1} with an ~38.9% population indicating that all the Td Fe^{2+} of **1a** and the impurity phase have been oxidized to Fe^{3+} through the oxidative removal of ~0.87 Na-ions from ~62% of $Na_{2.87}FeGaS_4$ and one Na from ~38% of $Na_3Fe_2S_4$ impurity. In that case, our achievable capacity should be 77.7 mAh/g [(83.02 mAh/g × 0.87 × 0.62) + (86.75 mAh/g × 0.38) = 77.7 mAh/g], which does not corroborate with the electrochemical charge curve since the experimentally observed capacity is only 63 mAh/g. The only likely explanation for this discrepancy could be that the oxidation of Fe^{2+} to Fe^{3+} continues to happen even when the charged cathode is removed and Mössbauer data is being collected for several days from 2 to 3 mg active mass. The spectrum of the discharged sample (Figure 5c) shows almost complete reversibility in the oxidation state of iron. The percentages of Fe^{2+} and Fe^{3+} in the discharged cathode, ~83.2 and 16.8%, respectively, with the IS and QS values of both Fe^{2+} and Fe^{3+} match very well with pristine (see Table 6). The close corroboration of percentage Fe^{3+} in pristine (13%) and discharged (16.8%) samples may indicate that it may not be possible to synthesize stoichiometric Na_3FeGaS_4 with all Fe in 2+, and a small amount of Fe^{3+} may be required to stabilize the structure. Along with a 96% reversal of the oxidation state of Fe in the Td site, we also observe that the impurity phase returns with its original chemical identity as evident by the IS and QS values of the impurity phase and its site population percentage in the reduced phase. From this observation, we can infer that the charge compensation during the electrochemical cycle is achieved by the $Fe^{2+/3+}$ redox of the Td site when cycled between 1.5−2.5 V. To achieve the full sodiated phase (Na_3FeGaS_4) from $Na_{2.87}FeGaS_4$ and study the polarization of the cathode, we performed GITT experiments at 10 mA/g current density. The experiment was carried out with a 60 min current pulse followed by either 240 or 120 min of relaxation time (Figures S4c and S4d). In both cases, the battery reached its equilibrium state during each relaxation step with very minimal polarization. Such a low polarization profile indicates the kinetically fast redox process of the cation ($Fe^{2+/3+}$) in intercalation type cathodes and full reversibility of Na (de)intercalation. However, the calculated specific capacity from the GITT experiments was matching exactly with our charge−discharge tests, and we were unable to achieve Na_3FeGaS_4 electrochemically (Figures S4e and S4f). This finding also supports the fact that it is probably not possible to stabilize a pure Fe^{2+} analogue of **1a** (Na_3FeGaS_4), an important observation that we missed in our previous publication due to the absence of Mössbauer data.[17]

Sodium Ion Conductivity. Realizing that Fe in $Na_xFeGaSe_4$ can be in mixed valent, $Fe^{2+/3+}$, we intended to introduce a vacancy in $Na_3ZnGaSe_4$ by substituting part of Zn with Fe and improve the ionic conductivity as a proof of concept. Indeed, our efforts have resulted in the formation of $Na_{2.79}Fe_{0.4}Zn_{0.6}GaSe_4$ (**3**), which is a sodium deficient phase charge compensated for by the Fe^{3+}. The ionic conductivity and activation energy were calculated using AC impedance measurements. The Nyquist plot in Figure 6 consists of a low frequency tail and a high frequency semicircle typical of chalcogenide-based sodium ion conductors. The equivalent circuit used and the related fitting parameters for room temperature ionic conductivity are detailed in Table S3. The temperature dependent ionic conductivity measured from

https://doi.org/10.1021/acs.inorgchem.4c00927
Inorg. Chem. 2024, 63, 11628−11638

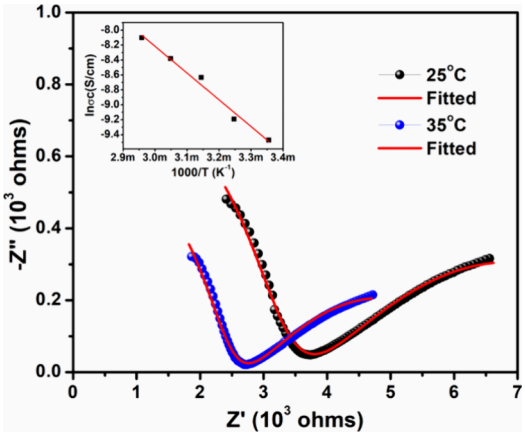

Figure 6. Nyquist plot for room temperature ionic conductivity of compound **3** (inset). The activation energy calculated from the experimental ionic conductivity vs temperature.

room temperature to 65 °C follows the Arrhenius behavior. The activation energy is calculated using $\sigma_T = \sigma_o \exp(-E_a/k_BT)$ where σ_T is the ionic conductivity, σ_o is a pre-exponential factor, T is the absolute temperature, and k_B is the Boltzmann constant. The room temperature ionic conductivity shows a value of 0.077 mS/cm with an activation energy of 0.30 eV. The ionic conductivity is comparable to our previously reported isostructural high ionic conductor compound, $Na_3ZnGaSe_4$ (0.12 mS/cm at 30 °C).[29] Slightly lower ionic conductivity of $Na_{2.79}Fe_{0.4}Zn_{0.6}GaSe_4$ could be due to the difference in the ionic radii $Fe^{2+/3+}$ vs Zn^{2+} or particle sizes or difference in electrode fabrication. A good intrinsic ionic conductivity coupled with moderate electrochemistry makes this class of compounds attractive for further tuning of the composition to improve the performance.

CONCLUSIONS

Three new quaternary selenides Na_xMGaQ_4 (M = Mn, Fe, mixed Zn/Fe) are successfully synthesized. The single crystal X-ray diffraction studies show a split Na-site for the Na_xMGaSe_4 (M = Fe and Zn/Fe) phases. Previously published sulfide analogues of iron, Na_3FeGaS_4, have been revisited with new findings of mixed valency, Na-vacancy, and facile Na-ion redox chemistry. The reversible Na ion (de)intercalation at a high current rate is well sustained in the sulfide analogue compared to the selenide (98% capacity retention in $Na_{2.87}FeGaS_4$ vs 72% capacity retention in $Na_{2.5}FeGaSe_4$). Mössbauer spectroscopic data reveal the involvement of the Fe^{2+} to Fe^{3+} redox couple for the charge compensation during the electrochemical cycles of $Na_{2.87}FeGaS_4$, when limited to a smaller voltage window, 1.5−2.5 V. $Na_{2.79}Zn_{0.6}Fe_{0.4}GaSe_4$ shows a reasonably high room temperature Na-ion conductivity of 0.077 mS/cm with an activation energy of 0.30 eV. Magnetic measurements on $Na_{2.87}FeGaS_4$ (**1a**) and $Na_3MnGaSe_4$ (**4**) show FC-ZFC divergence indicating the presence of spin-glass like transition with a high negative Weiss constant reveals the presence of geometrical magnetic frustration in these compounds due to the tetrahedral magnetic lattice. Currently, we are exploring substitution of various transition metals with an active redox couple to access both cation and anion redox in quaternary chalcogenide materials.

ASSOCIATED CONTENT

Supporting Information

The Supporting Information is available free of charge at https://pubs.acs.org/doi/10.1021/acs.inorgchem.4c00927.

Figures showing PXRD of Na_xMGaQ_4, Na ion coordination, dQ/dV plot, GITT plot, PXRD, and CV of Na_xFeGaQ_4, PXRD of $Na_{2.87}FeGaS_4$ after first charge and discharge. Tables of Atomic coordinates and isotropic thermal displacement parameters, equivalent circuit, fitted Mössbauer parameters and equivalent circuit fitting parameters for $Na_{2.79}Zn_{0.6}Fe_{0.4}Se_4$ (PDF)

Accession Codes

CCDC 2296323−2296326 and 2337943−2337945 contain the supplementary crystallographic data for this paper. These data can be obtained free of charge via www.ccdc.cam.ac.uk/data_request/cif, or by emailing data_request@ccdc.cam.ac.uk, or by contacting The Cambridge Crystallographic Data Centre, 12 Union Road, Cambridge CB2 1EZ, UK; fax: +44 1223 336033.

AUTHOR INFORMATION

Corresponding Author

Amitava Choudhury − *Department of Chemistry, Missouri University of Science and Technology, Rolla, Missouri 65409, United States;* orcid.org/0000-0001-5496-7346; Email: choudhurya@mst.edu

Authors

Santhoshkumar Sundaramoorthy − *Department of Chemistry, Missouri University of Science and Technology, Rolla, Missouri 65409, United States;* orcid.org/0000-0001-5037-0016

Srikanth Balijapelly − *Department of Chemistry, Missouri University of Science and Technology, Rolla, Missouri 65409, United States;* orcid.org/0000-0003-2720-8568

Sudip Mohapatra − *Department of Chemistry, Missouri University of Science and Technology, Rolla, Missouri 65409, United States;* Present Address: Kurseong College (affiliated under North Bengal University), Department of Chemistry, Kurseong, Darjeeling, West Bengal, PIN-734203, India; orcid.org/0000-0002-4317-5551

Sutapa Bhattacharya − *Department of Chemistry, Missouri University of Science and Technology, Rolla, Missouri 65409, United States;* orcid.org/0000-0001-6591-6624

Kartik Ghosh − *Department of Physics, Astronomy and Materials Science and Center for Applied Science and Engineering, Missouri State University, Springfield, Missouri 65897, United States*

Complete contact information is available at: https://pubs.acs.org/10.1021/acs.inorgchem.4c00927

Notes

The authors declare no competing financial interest.

ACKNOWLEDGMENTS

AC, SBs, and SS acknowledge the National Science Foundation (NSF) under grant number DMR- 1809128 for the funding of this work.

REFERENCES

(1) Sheldrick, W. S.; Wachhold, M. Chalcogenidometalates of the Heavier Group 14 and 15 Elements. *Coord. Chem. Rev.* **1998**, *176* (1), 211−322.

(2) Bensch, W.; Kanatzidis, M. Chalcogenides and Chalcogenidometalates: From Basic Research to Applications. *Z. Anorg. Allg. Chem.* **2012**, *638* (15), 2384−2385.

(3) Malliakas, C. D.; Kanatzidis, M. G. Inorganic Single Wall Nanotubes of $SbPS_{4-X}Se_x$ ($0 \leq x \leq 3$) with Tunable Band Gap. *J. Am. Chem. Soc.* **2006**, *128* (20), 6538−6539.

(4) Choudhury, A.; Dorhout, P. K. An Ordered Assembly of Filled Nanoscale Tubules of Europium Seleno-Silicate in the Crystal Structure of a Quaternary Compound. *J. Am. Chem. Soc.* **2007**, *129* (30), 9270−9271.

(5) Choudhury, A.; Grandjean, F.; Long, G. J.; Dorhout, P. K. $Na_{1.515}EuGeS_4$, A Three-Dimensional Crystalline Assembly of Empty Nanotubules Constructed with Europium(II/III) Mixed Valence Ions. *Inorg. Chem.* **2012**, *51* (21), 11779−11786.

(6) Tang, J.; Wang, X.; Zhang, J.; Wang, J.; Yin, W.; Li, D. S.; Wu, T. A Chalcogenide-Cluster-Based Semiconducting Nanotube Array with Oriented Photoconductive Behavior. *Nat. Commun.* **2021**, *12* (1), 1−8.

(7) Poudeu, P. F. P.; Takas, N.; Anglin, C.; Eastwood, J.; Rivera, A. $Fe_xPb_{4-X}Sb_4Se_{10}$: A New Class of Ferromagnetic Semiconductors with Quasi 1D $\{Fe_2Se_{10}\}$ Ladders. *J. Am. Chem. Soc.* **2010**, *132* (16), 5751−5760.

(8) Ranmohotti, K. G. S.; Djieutedjeu, H.; Lopez, J.; Page, A.; Haldolaarachchige, N.; Chi, H.; Sahoo, P.; Uher, C.; Young, D.; Poudeu, P. F. P. Coexistence of High-Tc Ferromagnetism and n-Type Electrical Conductivity in $FeBi_2Se_4$. *J. Am. Chem. Soc.* **2015**, *137* (2), 691−698.

(9) Zhou, Y.; Xing, L.; Finkelstein, G. J.; Gui, X.; Marshall, M. G.; Dera, P.; Jin, R.; Xie, W. $Cr_{2.37}Ga_3Se_8$: A Quasi-Two-Dimensional Magnetic Semiconductor. *Inorg. Chem.* **2018**, *57* (22), 14298−14303.

(10) Cava, R.; De Leon, N.; Xie, W. Introduction: Quantum Materials. *Chem. Rev.* **2021**, *121* (5), 2777−2779.

(11) Greedan, J. E. Geometrically Frustrated Magnetic Materials. *J. Mater. Chem.* **2001**, *11* (1), 37−53.

(12) Gardner, J. S.; Gingras, M. J. P.; Greedan, J. E. Magnetic Pyrochlore Oxides. *Rev. Mod. Phys.* **2010**, *82* (1), 53−107.

(13) Balents, L. Spin Liquids in Frustrated Magnets. *Nature* **2010**, *464* (7286), 199−208.

(14) Gingras, M. J. P.; McClarty, P. A. Quantum Spin Ice: A Search for Gapless Quantum Spin Liquids in Pyrochlore Magnets. *Rep. Prog. Phys.* **2014**, *77* (5), 056501.

(15) Broholm, C.; Cava, R. J.; Kivelson, S. A.; Nocera, D. G.; Norman, M. R.; Senthil, T. Quantum Spin Liquids. *Science* **2020**, *367* (6475), eaay0668.

(16) Chamorro, J. R.; McQueen, T. M.; Tran, T. T. Chemistry of Quantum Spin Liquids. *Chem. Rev.* **2021**, *121* (5), 2898−2934.

(17) Mohapatra, S.; Adhikary, A.; Ghosh, K.; Choudhury, A. Magnetically Frustrated Quaternary Chalcogenides with Interpenetrating Diamond Lattices. *Inorg. Chem.* **2017**, *56* (14), 7650−7656.

(18) Poudeu, P. F. P.; Djieutedjeu, H.; Ranmohotti, K. G. S.; Makongo, J. P. A. M.; Takas, N. Geometrical Spin Frustration and Ferromagnetic Ordering in $(Mn_XPb_{2-x})Pb_2Sb_4Se_{10}$. *Inorg. Chem.* **2014**, *53* (1), 209−220.

(19) Balijapelly, S.; Zhang, Q.; Sandineni, P.; Adhikary, A.; Mohapatra, S.; Sundaramoorthy, S.; Gerasimchuck, N.; Chernatynskiy, A. v.; Choudhury, A. High Sodium-Ion Conductivity in Interlocked Quaternary Chalcogenides Built with Supertetrahedral Building Units. *ACS Appl. Energy Mater.* **2021**, *4* (8), 7942−7951.

(20) Han, S.; Seo, J. Y.; Park, W. B.; Ikhe, A. B.; Choi, S. Y.; Han, S. C.; Sohn, K.-S.; Pyo, M. Vacancy-Controlled Quaternary Sulfide $Na_{3-x}Zn_{1-x}Ga_{1+x}S_4$ with Improved Ionic Conductivity and Aqueous Stability. *J. Mater. Chem. A* **2022**, *10* (47), 25039−25046.

(21) Schewe-Miller, I. *Metallreiche Hauptgruppenmetall-Chalkogenverbindungen: Synthese, Strukturen Und Eigenschaften*, Ph.D. Thesis, 1990.

(22) Balijapelly, S.; Sandineni, P.; Adhikary, A.; Gerasimchuk, N. N.; Chernatynskiy, A. V.; Choudhury, A. Ternary Alkali Ion Thiogallates, A_5GaS_4(A = Li and Na), with Isolated Tetrahedral Building Units and Their Ionic Conductivities. *Dalton Trans.* **2021**, *50* (21), 7372−7379.

(23) *Bruker- SAINT and SADABS, and SHELXTL*; Bruker AXS Inc., Madison, Wisconsin, USA, 2008.

(24) Sheldrick, G. M. A Short History of SHELX. *Acta Crystallogr. A* **2008**, *64* (1), 112−122.

(25) Hübschle, C. B.; Sheldrick, G. M.; Dittrich, B. ShelXle: A Qt Graphical User Interface for SHELXL. *J. Appl. Crystallogr.* **2011**, *44* (6), 1281−1284.

(26) Klepp, K.; Boller, H. $Na_3Fe_2S_4$, Ein Thioferrat Mit Gemischt Valenter Sk∞/1[FeS2]-Kette. *Monatshefte für Chemie* **1981**, *112* (1), 83−89.

(27) Klepp, K. O.; Sparlinek, W. Crystal Structure of Trisodiumtetraselenodiferrate, $Na_3Fe_2Se_4$. *Z. Kristallogr Cryst. Mater.* **1996**, *211* (9), 626−626.

(28) Lagarec, K.; Rancourt, D. G. Extended Voigt-Based Analytic Lineshape Method for Determining N-Dimensional Correlated Hyperfine Parameter Distributions in Mössbauer Spectroscopy. *Nucl. Instrum Methods Phys. Res. B* **1997**, *129* (2), 266−280.

(29) Kienle, L.; Deiseroth, H. J. Crystal Structure of Sodium Trigallium Pentaselenide, $NaGa_3Se_5$. *Zeitschrift fur Kristallographie - New Crystal Structures* **1998**, *213* (1−4), 21−22.

(30) Kim, J.; Hughbanks, T. Synthesis and Structures of New Layered Ternary Manganese Selenides: $AMnSe_2$ (A = Li, Na, K, Rb, Cs) and $Na_2Mn_2Se_3$. *J. Solid State Chem.* **1999**, *146* (1), 217−225.

(31) Ensling, J.; Gütlich, P.; Spiering, H.; Klepp, K. Mössbauer and Magnetic Studies of Mixed-Valence Linear Chain Compounds: $Na_3Fe_2S_4$ and $Na_3Fe_2Se_4$. *Hyperfine Interact.* **1986**, *28* (1−4), 599−601.

(32) Reiff, W. M.; Grey, I. E.; Fan, A.; Eliezer, Z.; Steinfink, H. The Oxidation State of Iron in Some BaFeS Phases: A Mössbauer and Electrical Resistivity Investigation of Ba_2FeS_3, $Ba_7Fe_6S_{14}$, $Ba_6Fe_8S_{15}$, $BaFe_2S_3$, and $Ba_9Fe_{16}S_{32}$. *J. Solid State Chem.* **1975**, *13* (1−2), 32−40.

(33) Reiff, W. M.; Grey, I. E.; Fan, A.; Eliezer, Z.; Steinfink, H. The Oxidation State of Iron in Some BaFeS Phases: A Mössbauer and Electrical Resistivity Investigation of Ba_2FeS_3, $Ba_7Fe_6S_{14}$, $Ba_6Fe_8S_{15}$, $BaFe_2S_3$, and $Ba_9Fe_{16}S_{32}$. *J. Solid State Chem.* **1975**, *13* (1−2), 32−40.

(34) Villain, J. Insulating Spin Glasses. *Zeitschrift für Physik B Condensed Matter and Quanta* **1979**, *33* (1), 31−42.

(35) Binder, K.; Young, A. P. Spin Glasses: Experimental Facts, Theoretical Concepts, and Open Questions. *Rev. Mod. Phys.* **1986**, *58* (4), 801−976.

(36) Whittingham, M. S. Chemistry of Intercalation Compounds: Metal Guests in Chalcogenide Hosts. *Prog. Solid State Chem.* **1978**, *12*, 41.

(37) Lee, E.; Lee, W. C.; Asl, N. M.; Kim, D.; Slater, M.; Johnson, C.; Kim, Y. Reversible $NaVS_2$ (De)Intercalation Cathode for Na-Ion Batteries. *ECS Electrochemistry Letters* **2012**, *1* (5), A71−A73.

(38) Shadike, Z.; Zhou, Y. N.; Chen, L. L.; Wu, Q.; Yue, J. L.; Zhang, N.; Yang, X. Q.; Gu, L.; Liu, X. S.; Shi, S. Q.; Fu, Z. W. Antisite Occupation Induced Single Anionic Redox Chemistry and Structural Stabilization of Layered Sodium Chromium Sulfide. *Nat. Commun.* **2017**, *8* (1), 1−9.

(39) Wang, T.; Ren, G. X.; Shadike, Z.; Yue, J. L.; Cao, M. H.; Zhang, J. N.; Chen, M. W.; Yang, X. Q.; Bak, S. M.; Northrup, P.; Liu, P.; Liu, X. S.; Fu, Z. W. Anionic Redox Reaction in Layered NaCr2/3Ti1/3S2 through Electron Holes Formation and Dimerization of S−S. *Nat. Commun.* **2019**, *10* (1), 4458.

(40) Leube, B. T.; Salager, E.; Chesneau, E.; Rousse, G.; Vezin, H.; Abakumov, A. M.; Tarascon, J. M. Layered Sodium Titanium Trichalcogenide Na_2TiCh_3 Framework (Ch = S, Se): A Rich Crystal and Electrochemical Chemistry. *Chem. Mater.* **2022**, *34* (5), 2382−2392.

(41) Shi, D. R.; Shadike, Z.; Wang, T.; Yang, S. Y.; Xia, H. Y.; Wang, Y. K.; Yue, J. L.; Hu, E.; Bak, S. M.; Yue, X. Y.; Zhou, Y. N.; Ma, L.; Ghose, S.; Wu, T.; Zhang, Q. H.; Xing, Z.; Zhang, Y. N.; Zheng, L.; Gu, L.; Yang, X. Q.; Fu, Z. W. Reversible Dual Anionic-Redox

https://doi.org/10.1021/acs.inorgchem.4c00927
Inorg. Chem. 2024, 63, 11628−11638

Chemistry in NaCrSSe with Fast Charging Capability. *J. Power Sources* **2021**, *502*, 230022.

https://doi.org/10.1021/acs.inorgchem.4c00927
Inorg. Chem. 2024, 63, 11628−11638